Metallomics

RSC Publishing

PAPER

View Article Online
View Journal

Cite this: DOI: 10.1039/c3mt00215b

Thlaspi arvense binds Cu(II) as a bis-(L-histidinato) complex on root cell walls in an urban ecosystem†

Alain Manceau,‡*[a] Alexandre Simionovici,[a] Martine Lanson,[a] Jonathan Perrin,[a] Rémi Tucoulou,[b] Sylvain Bohic,[bc] Sirine C. Fakra,[d] Matthew A. Marcus,[d] Jean-Philippe Bedell[e] and Kathryn L. Nagy[f]

Received 8th August 2013,
Accepted 14th October 2013

DOI: 10.1039/c3mt00215b

www.rsc.org/metallomics

Root cell walls accumulate metal cations both during acquisition from the environment and removal from the protoplast to avoid toxicity, but molecular forms of the metals under field conditions remain elusive. We have identified how copper is bound to cell walls of intact roots of native *Thlaspi arvense* by combining synchrotron X-ray fluorescence and absorption techniques (XANES and EXAFS) at the nano-, micro-, and bulk scales. The plants grew naturally in sediment in a stormwater runoff basin at copper concentrations typical of urban ecosystems. About 90% of acquired copper is bound *in vivo* to cell walls as a unique five-coordinate Cu(II)–bis(L-histidinato) complex with one L-histidine behaving as a tridentate ligand (histamine-like chelate) and the other as a bidentate ligand (glycine-like chelate). Tridentate binding of Cu(II) would provide thermodynamic stability to protect cells against copper toxicity, and bidentate binding may enable kinetic lability along the cell wall through protein–protein docking with the non-bonded imidazole group of histidine residues. EXAFS spectra are provided as ESI† to facilitate further identification of Cu–histidine and distinction of Cu–N from Cu–O bonds in biomolecules.

Introduction

The multiple roles of copper in biochemical reactions result from the redox-sensitivity of the Cu^{2+}/Cu^{+} couple, which has elevated standard electrode potentials when complexed in proteins that facilitate electron transfer in cellular processes.[1] Imbalances in cellular copper are implicated in multiple diseases that strike eukaryotic organisms. In plants, copper is essential for photosynthesis, mitochondrial respiration, lignin synthesis, root growth, ethylene sensing, and reactive oxygen metabolism.[2,3] Typically, the concentration of nutrient copper falls between 5 and 30 mg kg^{-1} dry weight (DW) in vegetative tissues, regardless of the copper concentration of the soil in which the plant grows.[4] When in excess, copper can catalyze the production of hydroxyl radicals, with subsequent damage to macromolecules involved in the production (chloroplasts) and storage (mitochondria) of energy, to protein synthesis, and to biomembranes through the peroxidation of unsaturated fatty acids.[5–9] To maintain nutrient requirements, while simultaneously protecting photosynthetic and reproductive tissues from excess amounts, vascular plants have evolved physiological mechanisms to regulate the concentration of copper in root cells and its transport in vascular bundles (*i.e.*, xylem sap) from the stele.[10–13]

Knowledge of the location and molecular forms of copper in the root is sparse, especially at non-toxic concentrations. This information is critical for developing approaches to preserve copper homeostasis in plants as environmental conditions change, and for applying phytotechnology to remediate contaminated soil and water.[14,15] Results of previous electron microscopy studies show that copper is dominantly contained on cell walls as are other metals.[16–19] Copper may enter the cell wall through intercellular spaces during the uptake of water from the environment, and as a result of trace metal removal from the protoplast during the sequestration process for detoxifying excess copper. Inside cells, copper typically is not sequestered in root cortical vacuoles, as is commonly the case for zinc and cadmium detoxification.[20–22] Sequestration of copper in vacuoles has been observed only in two Cu-tolerant plants, *Armeria maritima* sp. halleri grown in the wild on Zn-polluted soil with a root content

[a] *ISTerre, CNRS and University of Grenoble, Grenoble 38041, France*
[b] *European Synchrotron Radiation Facility (ESRF), BP220, Grenoble 38043, France*
[c] *Inserm U-836, Grenoble Institut des Neurosciences (GIN), Grenoble 38042, France*
[d] *Advanced Light Source, Lawrence Berkeley National Laboratory, Berkeley, CA 94720, USA*
[e] *Laboratoire d'Ecologie des Hydrosystèmes Naturels et Anthropisés (LEHNA), ENTPE, CNRS and University of Lyon 1, Vaulx-en-Velin 69518, France*
[f] *Department of Earth and Environmental Sciences, University of Illinois at Chicago, Chicago, IL 60607, USA*

† Electronic supplementary information (ESI) available: File S1: Results and figures. File S2: Cu K-edge EXAFS spectra of the cell wall and model compounds. See DOI: 10.1039/c3mt00215b

‡ ISTerre, Maison des Géosciences, Domaine Universitaire, BP 53, 38041 Grenoble Cedex 9, France. E-mail: alain.manceau@ujf-grenoble.fr; Tel: +33 4 76 63 51 93.

of 220 mg Cu kg^{-1} DW,[23] and *Elsholtzia splendens*, a native species at copper mines in central China,[24] grown hydroponically with added metal at an uncommonly high root content of 2288 mg Cu kg^{-1} DW.[25] Roots from *E. splendens* with even higher added copper concentrations of 12–14 $\times 10^3$ mg kg^{-1} DW contained O, N and S copper-binding ligands identified from bulk X-ray absorption near edge structure (XANES) spectra. Hydroxyl and carboxyl-type oxygen ligands (40–60%) were inferred to bind copper on cell walls, histidine-type nitrogen ligands (30–50%) were assigned to xylem sap, and glutathione-type sulfur ligands ($\sim$10%) were allocated to the cytoplasm.[26]

To address the complex relationships between plants and their environment, X-ray measurements on natural systems or from outdoor experiments are needed. Using this approach, we showed previously that divalent copper is reduced to the metallic state in a mycorrhizal association in soil.[27] Here, we report that it is now possible to resolve copper complexes in native plants by chemical and structural analysis of undisrupted root tissue at sub-cellular to multi-cellular scales using combined synchrotron nanoscale, microscale, and bulk techniques. Results were obtained for naturally grown *Thlaspi arvense* (field pennycress), a common and edible annual ruderal Brassicaceae (Cruciferae) that is Cu-sensitive and therefore a good proxy for understanding how common dicotyledonous plants cope with moderate metal contamination in urban ecosystems. This plant is also used in comparative anatomy and physiology studies of the model (Zn,Cd)-hyperaccumulator *Thlaspi caerulescens* (renamed *Noccaea caerulescens*).[28–30] Cellular preservation, especially of highly vacuolated cortical cells, was achieved by high-pressure freezing techniques and ultramicrotomic sectioning.[31–34] Although freezing of biological tissues under *in vivo* conditions has been applied to micro-scale imaging of metals in root tissues,[35,36] this report is the first of metal imaging inside cells at high-resolution with a nano X-ray beam. Cryogenic temperature was applied to prevent X-ray radiation damage,[37,38] and the results verified at two beamlines: the high-flux undulator beamline ID22 at the European Synchrotron Radiation Facility (ESRF) and the low-flux bending magnet beamline 10.3.2 at the Advanced Light Source (ALS).[39,40] Results show that at concentrations of 50–100 mg kg^{-1} DW in natural plants, Cu accumulates in the walls of both cortical and stellar root cells, and is bound to oxygen and nitrogen donors from histidine residues, not to carboxylic ligands from pectins, as previously hypothesized by analogy to moss and fern.[41–43]

Experimental

Sampling site and plant material

Eight specimens of the same size of *T. arvense* were harvested in April before the blooming season from the stormwater runoff basin "Django-Reinhardt" east of Lyon (45N 44.163′; 4E 57.478′). This basin receives water from a light industrial suburb watershed of 185 ha. The stormwater runoff basin first enters a forebay at the inlet where the larger solids and coarse organic material settle out. The detention basin is connected through a concrete spillway to an 8000 m^2 infiltration basin developed over glacially-derived alluvial deposits from the Rhône river. The incoming water initially flows through a marsh colonized spontaneously by invasive wetland species, mainly *Phalaris arundinacea* and *Polygonum mite*. Then the surface water meanders back and forth on its way through the system while infiltrating into the ground. The semi-dry area located downstream is colonized by ruderal plants, such as *Senecio inaequidens*, *Erigeron annuus*, *Capsella bursa pastoris*, and *Cardamine Hirsuta*. The semi-xerophile *T. arvense* is also observed during the spring in this area, but is easily outcompeted by other plants.

The sediment colonized by *T. arvense* contains 190–220 mg kg^{-1} DW of Cu, 900–1200 mg kg^{-1} DW of Zn, and 35–120 mg kg^{-1} DW of Ni.[44,45] The metal contents are comparable to those for sediments in stormwater ponds at other similar urban locations,[46,47] and mostly higher than the Severe Effect Levels (SEL) of 110 mg kg^{-1} DW of Cu, 270–820 mg kg^{-1} DW of Zn, and 50–75 mg kg^{-1} DW of Ni defined for sediment quality by the Ministry of the Environment of Ontario, Canada[48] and the New York State Department of Environmental Conservation.[49] Copper may be phytotoxic at these concentrations and affect plant growth through oxidative stress with chlorosis symptoms.[50–54]

The plants were potted in the field with their intact rhizospheric soil and transported to the laboratory in May 2011. There, leaves were collected and primary (Rp) and secondary (Rs) roots were separated from the soil, washed with purified water (Milli-Q reagent grade), cleansed of adhered soil particles, and split into three batches. Split I was freeze-dried and stored for chemical analysis. Split II was used for bulk Cu K-edge extended X-ray absorption fine structure (EXAFS) spectroscopy. The living roots of Split II were immediately plunged into liquid nitrogen and preserved frozen until measurement. Split III was used for *in situ* synchrotron X-ray nano-fluorescence (nano-SXRF) and micro-XANES and micro-EXAFS spectroscopy.[37,55–60] Fragments of live secondary roots were cryofixed with a high pressure freeze fixation apparatus (Leica EM HPM100). The frozen hydrated samples were subsequently dehydrated with acetone and 0.1% uranyl acetate at −90 °C, and then ramped progressively to −50 °C for embedding in Lowicryl resin (Electron Microscopy Sciences). The resin was polymerized under ultraviolet light at −50 °C for 48 hours and at 20 °C for 48 hours. The dried root samples were taken out of the cryo-chamber and sectioned into 2 μm-thick slices at room temperature. The best sections were deposited on Si_3N_4 windows for synchrotron analyses, and others on glass slides, stained with toluidine blue, and examined under a light microscope for morphological and histological control (ESI,† Fig. S1).

Chemical analysis

The roots and leaves were analyzed for total Cu and Zn concentration as follows. Freeze-dried roots and leaves from Split I were ground using a centrifugal mill and 50 to 100 mg reacted in Savillex PFA-flasks. The roots were reacted initially with 10 drops of 30% H_2O_2 and the suspension evaporated at 70 °C until a single drop was left. The drop was resuspended with 2–4 mL 7 N HNO_3 and reacted at 95 °C until completely digested.

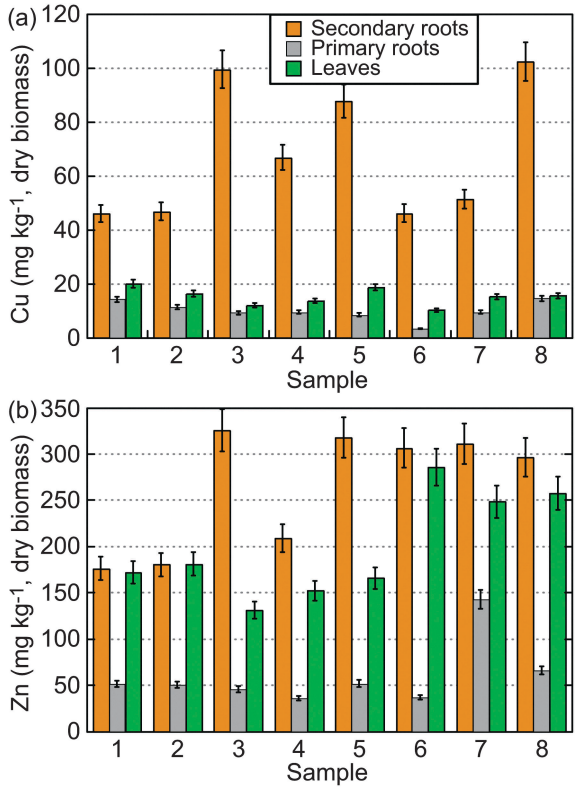

Fig. 1 Cu (a) and Zn (b) contents in secondary roots, primary roots, and leaves of eight specimens of *Thlaspi arvense*.

The last drop of residue was re-dissolved in 10 to 12 mL 2% HNO_3. Solutions and standards, both in 2% HNO_3, were analyzed by Inductively Coupled Plasma Optical Emission Spectrometry (Perkin-Elmer Optima 3300DV ICP-OES). The analytical precision from replicates was better than 3.2%, and the total experimental precision obtained by propagating the errors in the solubilization steps and analysis was estimated to be 7%. Concentrations reported in Fig. 1 were calculated on a freeze-dried weight basis.

Preparation of solution complexes used as model compounds

A 16 mM $Cu(SO_4)\cdot 5H_2O$ stock solution in Milli-Q water was used as the source of Cu^{2+} for the aquo complexes. Two L-histidine complexes were prepared at [Cu] = 4 mM, a Cu : ligand (Cu : L) ratio of 1 : 4, and pH 4.8 and 7.4; three nicotianamine (NA, T. Hasegawa Co., LTD) complexes at [Cu] = 4 mM, Cu : L = 1 : 4 and pH 4.8, Cu : L = 1 : 1 and pH 6.5, and Cu : L = 1 : 5 and pH 7.4; one glycine, one glutamate, and one proline complex all at [Cu] = 5 mM, Cu : L = 1 : 8 and pH 7.4, and one thiolactate complex at [Cu] = 4 mM, Cu : L = 1 : 50 and pH 11.0. The pH was maintained at 4.8 with an acetate buffer, and at 6.5 and 7.4 with a phosphate buffer (KH_2PO_4–Na_2HPO_4). All model complexes were prepared the day before the X-ray absorption experiment and recorded in the frozen state. Formation of ice crystals during freezing was prevented by adding 30% (v/v) glycerol as a glassing agent. The three Cu–NA EXAFS spectra were statistically identical, as previously reported for this type of complex.[61]

SXRF measurements and data analysis

The nano-SXRF maps from sample split III were recorded at room temperature on the undulator ID22-EH2 nanoprobe at the ESRF. The incident energy was 17 keV with 1.5% bandwidth (PINK beam mode), and the X-ray beam focused to 69 × 77 nm^2, Vertical × Horizontal Full Width at Half Maximum (V × H FWHM), using Kirkpatrick–Baez multilayer optics. The total flux was 3 × 10^8 photons per s.[39] Coarse and fine maps were recorded at scanning resolutions from 2.0 × 2.0 μm^2 down to 0.18 × 0.18 μm^2 and 200 ms counting time per pixel. The fluorescence-line interferences were resolved with the fitting program PyMCA (ESI,† Fig. S2).[62] The grayscale maps from Fig. 2 are the pixel intensities of the Cu Kα and Zn Kα lines.

XANES and EXAFS measurements and data analysis

Cu K-edge bulk X-ray absorption spectra of the frozen-hydrated (split II) roots (Rs and Rp) and frozen aqueous complexes were recorded at liquid helium temperature (LHe, 8 to 16 K) at beamline BM30B (FAME) of the ESRF. On this beamline, the photon flux is 5 × 10^{11} photons per s for 200 mA in a beam spot size of 100 × 300 μm^2, V × H FWHM.[63] Micro X-ray absorption spectra cannot be recorded currently at LHe temperature, and so, were acquired at liquid nitrogen temperature (LN_2, < 100 K) on two X-ray microprobes for measurement quality assessment. One series of measurements was performed on the bending magnet microprobe 10.3.2 at the ALS, and another on the undulator microprobe ID22-EH1 at the ESRF.[39,40] The first instrument produces at the Cu K-edge 5 × 10^9 photons s^{-1} in a spot size of 15 × 6 μm^2, V × H FWHM, and the second 2 × 10^{11} photons s^{-1} in a spot size of 1.5 × 4.5 μm^2, V × H FWHM; the flux density at ID22-EH1 (ESRF) is about 500 times higher than that at 10.3.2 (ALS). The sample was translated following each sweep to access fresh material, and caution was taken that all individual spectra looked identical before summing to improve statistics. The root samples were stable with respect to photo-reduction for the duration of a single scan at BM30B at LHe and 10.3.2 at 98 K. Radiation damage was avoided on ID22-EH1 by reducing the energy interval and scan time to 15 min per analyzed area. All spectra shown are free of radiation damage, such as the photoreduction of Cu^{2+} to Cu^+ and Cu^0 under the X-ray beam, or resultant artifactual complexation of Cu^+ to sulfur ligands.[64,65] The absolute energy of XANES spectra is referenced to the first inflection point of a Cu foil at 8980.3 eV. X-ray absorption data were analyzed by standard methods.[65]

Results

Copper accumulation in secondary roots

Copper concentration is seven times higher in secondary roots (Rs, 68.3 ± 24.6 mg kg^{-1} DW, n = 8) than in shoots (15.3 ± 3.3 mg kg^{-1} DW, n = 8), whereas zinc is more evenly distributed between the two organs (Rs = 265.6 ± 64.8 mg kg^{-1} DW; shoot = 199.5 ± 56.6 mg kg^{-1} DW) (Fig. 1). Woody primary roots have less copper (Rp = 10.0 ± 3.6 mg kg^{-1} DW, n = 8) and zinc (Rp = 60.4 ± 34.8 mg kg^{-1} DW, n = 8) than secondary roots, because

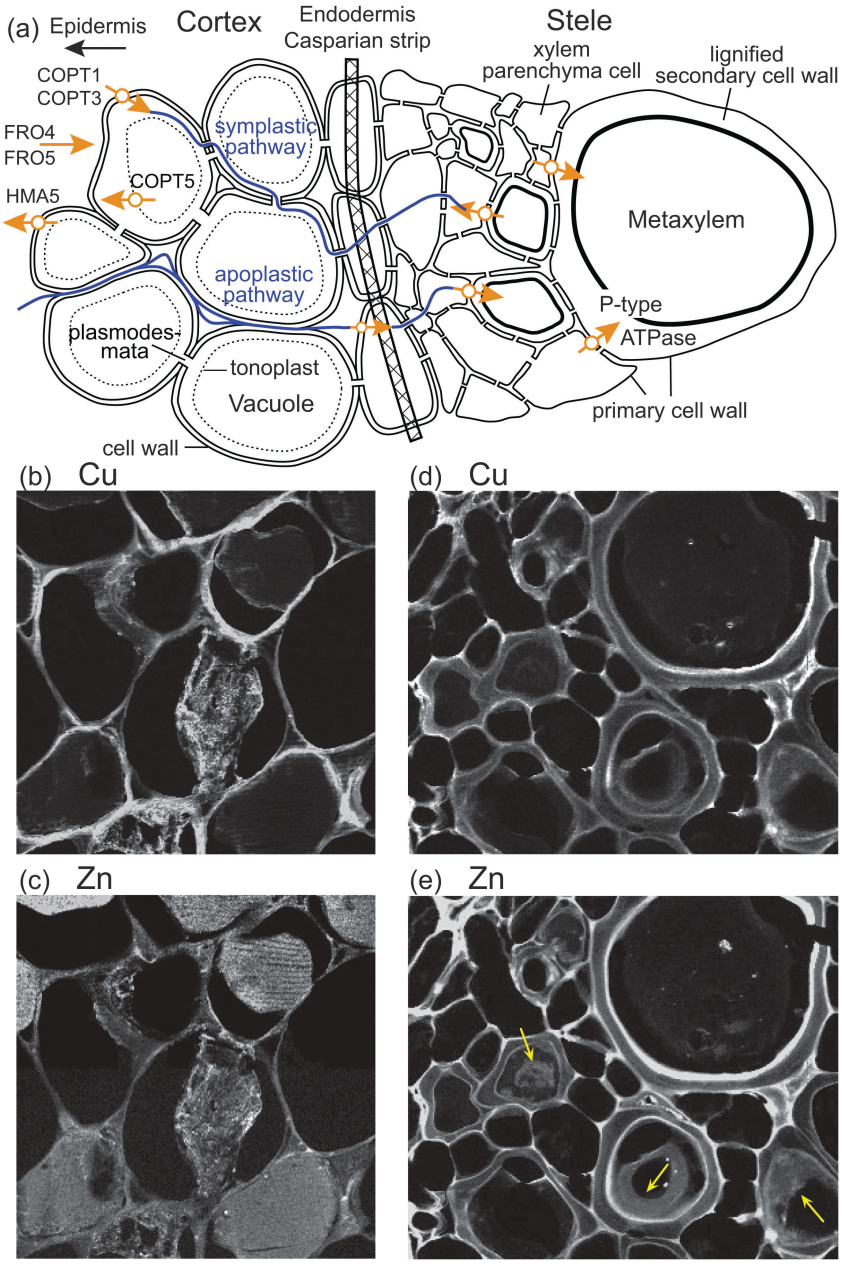

Fig. 2 (a) Schematic of radial pathways for metals in the root. Transport from the epidermis to the xylem vessels may occur symplastically through the cytoplasm of cells linked by plasmodesmata or apoplastically by diffusion through extracellular spaces or transport along the cell walls, skirting protoplasts. Apoplastic transport is interrupted by the lignified Casparian strip, forcing metals to cross the selectively permeable plasma membrane. Once in the root symplast, metals can be immobilized in vacuoles. Brown arrows indicate specific protein transporters involved in Cu uptake and homeostasis in cytoplasm.[11,101,102] (b–e) Nano-SXRF images of Cu and Zn (bright areas) in a secondary root of *Thlaspi arvense* obtained from the decomposition of the total X-ray fluorescence spectra (ESI,† Fig. S2).[62] (b and c) Cortical tissue showing compartmentation of Cu on cell walls and Zn in vacuoles and on cell walls. Image size: 54 (H) × 55 (V) μm^2, pixel size: 0.18 (H) × 0.18 (V) μm^2. (d and e) Stele with several protoxylem and metaxylem vessels with thickened walls encrusted with lignin (ESI,† Fig. S1). Cu and Zn occur on the cell wall and in the xylem lumen (yellow arrows). Image size: 63 (H) × 53 (V) μm^2, pixel size: 0.2 (H) × 0.2 (V) μm^2.

their main function is to transport water and nutrients from fine roots to the stem. Thus, the majority of the absorbed Cu is accumulated in secondary roots, and only a small fraction is translocated to aerial parts, as has been reported in other plants.[66–69] Resistance to anthropogenic emissions of copper occurs by the root accumulating an excess and then regulating the amount transported to the shoot. In contrast, zinc accumulates in roots and shoots[70–72] likely by storage in vacuoles in both below- and above-ground tissues.[22,73] We evaluate this difference in how *T. arvense* responds to copper and zinc intake next.

Distribution of Cu and Zn at the cellular scale

Nano-SXRF imaging of prepared sections from fine, soft secondary roots shows good ultrastructural preservation in localized areas

of the cortex and vascular cylinder, and capture of xylem sap (Fig. 2). Zinc is concentrated in cortical vacuoles and cell walls, whereas copper is mostly compartmented on cell walls.[74] Less than 5% of the copper is in vacuoles, as estimated from semi-quantitative SXRF analysis (ESI,† Fig. S2). Induced sequestration of copper in vacuoles was observed in the non-tolerant plants *Allium sativum* and *Oryza sativa* when exposed to excess copper in hydroponic nutrient solutions.[75,76] Here, *T. arvense* did not resort to significant vacuolar sequestration to control cytoplasmic copper, suggesting that the 50–80 mg kg^{-1} DW root concentration is not toxic, and therefore, copper stress at the sampling site can be alleviated by sequestration on cell walls.

The volume of each preserved cortical cell is almost fully occupied by a large vacuole and the cytoplasm is reduced to a thin parietal film (bottom of Fig. 2c). Some vacuoles have contracted and are not pressed against the cell wall in the cortex. The fragile plasma membrane probably was destroyed during preparation and as a result collapsed onto the tonoplast. Where plasma and vacuolar membranes both collapsed, the entire cell appears plasmolyzed (*i.e.*, dehydrated) and the attachment of the plasma membrane to plasmodesmata is revealed (middle cell of Fig. 2c). This completely deteriorated cell is an artifact, but gives a good view of the otherwise invisible endomembranes which would contain the copper and zinc transmembrane proteins that regulate metal homeostasis in the cytoplasm (Fig. 2a).

In the stele, the xylem parenchyma cells adjacent to protoxylem and metaxylem elements apparently lack vacuoles and appear empty in contrast to cortical parenchyma cells (Fig. 2d and e). Copper and zinc are mostly concentrated in the primary cell wall and the inner surface of the thick, lignified secondary cell wall (ESI,† Fig. S1). Diffuse Cu- and Zn-containing areas, which may be sap, occur in the xylem elements. Residual cytoplasm from immature xylem cells is unlikely, because the root

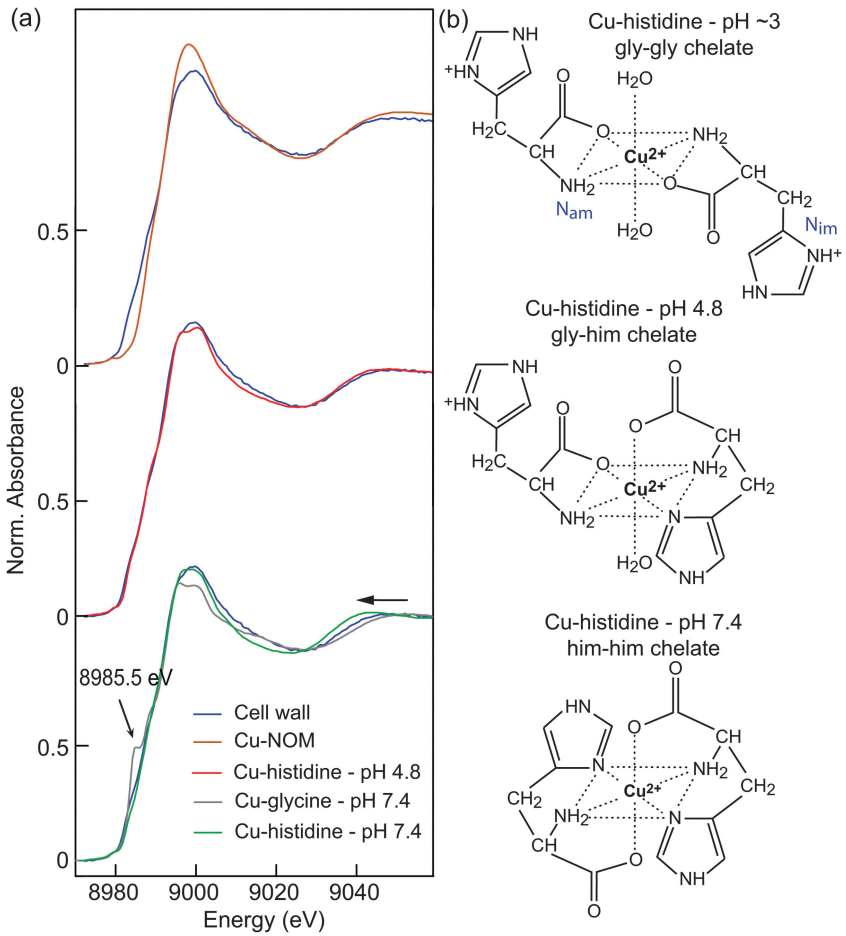

Fig. 3 Copper speciation by micro-XANES. (a) Micro-XANES spectra of Cu in cell walls from ultramicrotomic sections (Fig. 2) compared to bulk spectra from model compounds. (b) Molecular structures of Cu^{2+} complexes with histidine.[78] In natural organic matter (NOM), Cu^{2+} is coordinated to oxygen in carboxylic and hydroxyl groups (Elliott Soil humic acid).[65] The L-histidine ligand changes orientation with pH. At pH ~3.0, the major Cu^{2+} species is a bis-bidentate chelate in the equatorial plane through amine N (N_{am}) and carboxyl O atoms (gly–gly chelate). This complex co-exists with other species when histidine is used as a ligand, but is obtained in pure form with glycine at pH 7.4 (ESI,† Results). At pH 4.8, the major Cu^{2+} species with histidine is a bis-bidentate chelate formed of a five-membered glycine-like chelate and a six-membered histamine-like chelate through amine N and imidazole N (N_{im}) atoms. The carboxylate group displaced from the equatorial position occupies an axial site. At pH 7.4, the glycine-like chelate converts into a second histamine-like chelate and the two carboxyl O atoms align in an axial position, forming a double tridentate chelate. The leftward shift in energy at ~9040 eV (arrow at $k = 3.8$ $Å^{-1}$ on Fig. 4) accompanies the increase in average Cu–ligand distance in going from the gly–gly (2N + 2O ligands), to the gly–him (on cell wall; 3N + 1O), to the him–him (4N) configuration.

fragments were sectioned at least one centimeter from the meristematic root tip.

Copper binding to histidine in the cell wall

The micro-XANES spectrum of cell wall copper has an edge maximum at 8999 eV, the same energy as Cu^{2+} coordinated to carboxyl O in natural organic matter (NOM),[65] which is a proxy for Cu bound to OH and/or COOH groups in cellulose, lignin and pectin (Fig. 3a). A weak absorption on the rising part of the edge is discernible in the cell wall spectrum. This low-energy tail is absent in Cu^{2+}–(O,OH) model organic compounds and unrelated to photoreduction, but is typically present when Cu^{2+} is bonded to aminocarboxylate ligands.[77] An identical spectrum is observed for the model amino acid complex of Cu^{2+} chelated in solution at pH 4.8 with L-histidine (his) (Fig. 3b). Histidine can bind metals as a bidentate or a tridentate ligand at three sites: the carboxylate oxygen (O_c), the amino nitrogen (N_{am}), and the imidazole imido nitrogen (N_{im}) closest to the CH_2 group (ESI†). At pH 4.8, the dominant moiety is a Cu^{2+}–$N_{am}O_cN_{am}N_{im}$ bis-chelate formed of (1) a five-membered glycine-like (gly) bidentate chelate with N_{am} and O_c, and (2) a six-membered histamine-like (him) tridentate chelate with N_{am} and N_{im} in the equatorial plane and the second O_c in the axial position (gly–him chelate).[78] At pH below 4.8, histidine binds Cu^{2+} in a bisglycine-like $N_{am}O_cN_{am}O_c$ coordination with two water molecules in the axial position (gly–gly chelate) producing an absorption feature at 8985.5 eV not observed in the cell-wall spectrum. At circumneutral pH and above, the pH 4.8 Cu^{2+}–$N_{am}O_cN_{am}N_{im}$ bis-chelate changes into a $N_{am}N_{im}N_{am}N_{im}$ coordination with the two O_c atoms in the axial position (him–him chelate). Because the Cu–N distance is on average slightly longer than the Cu–O distance, the conversion from a mixed (O,N) to a full N coordination in the equatorial plane appears in the extended XANES region as a shift to lower energy (*i.e.*, longer bond distance) of the first EXAFS oscillation, also not observed in the data (Fig. 3 and 4).[78] Thus, the close match of the XANES spectrum of the pH 4.8 Cu^{2+}–his model complex with that of the cell wall supports a Cu^{2+}–gly–him type structure on the cell walls. Previously described O and S ligands[61,79–82] are incompatible models, because these ligands give distinctive XANES signals.[65]

The nature and geometry of the cell wall complex was further characterized by micro-EXAFS spectroscopy. The cell wall EXAFS spectrum is distinctly different from those of two

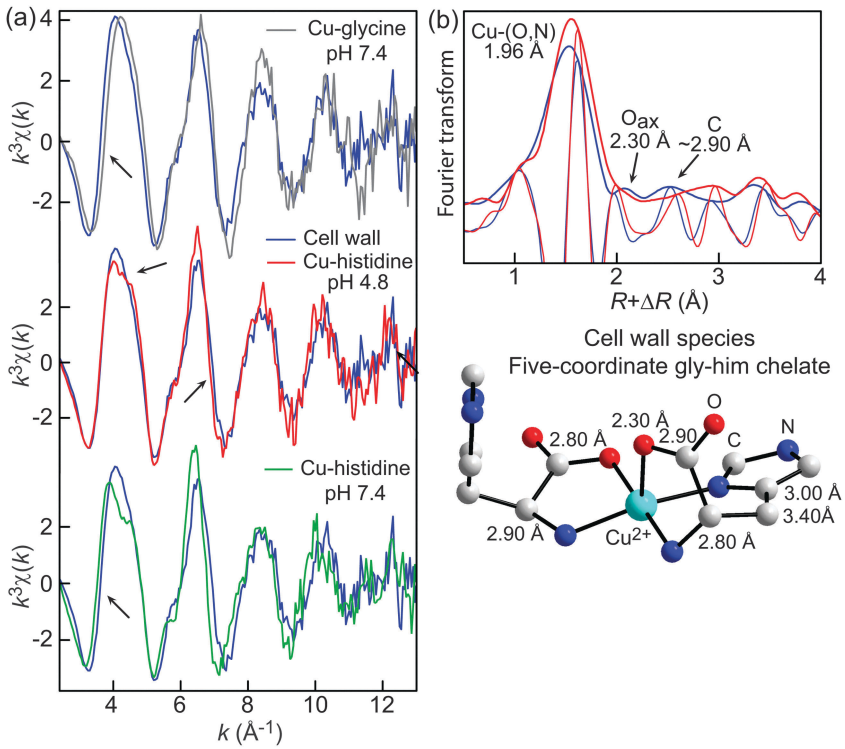

Fig. 4 Copper speciation by micro-EXAFS. (a) Micro-EXAFS spectra of Cu in cell walls from ultramicrotomic sections (Fig. 2) compared to bulk spectra from model compounds. Arrows highlight spectral differences. The spectrum of Cu–glycine at pH 7.4 is that of the pure $CuGly_2$ species (gly–gly chelate) which would exist in a mixture with a lesser amount of CuGly at pH 4.8. The gly–gly chelate cannot be obtained pure in a solution with histidine at pH 3 (ESI†). (b) Fourier transforms (modulus plus imaginary part) of the EXAFS spectra of the cell wall and gly–him chelate, and proposed structure for the cell wall complex. The imaginary parts of the Fourier transforms show that the first coordination shell (Cu–(O,N) peak) is at the same distance in the cell wall and the gly–him chelate, whereas it is shortened in gly–gly and expanded in him–him (ESI,† Results and Fig. S3). The structure, adapted from Deschamps *et al.*,[103] shows a neutral five-coordinate Cu^{2+} complex with bidentate and tridentate L-histidine ligands forming a distorted square planar pyramid. Folding the side carboxyl chain on top of the $Cu(O,N)_4$ plane decreases the range of the Cu–O_{ax} and Cu–C distances compared to the gly–gly configuration. The authenticity of the cell wall complex measured by micro-EXAFS was verified by measuring the bulk EXAFS spectra of fresh roots (Rs and Rp) rapidly frozen in liquid nitrogen and mounted in frozen-hydrated form into the helium cryostat from beamline BM30B (ESI,† Fig. S4). Spectroscopic data for roots and reference compounds are provided in the ESI.†

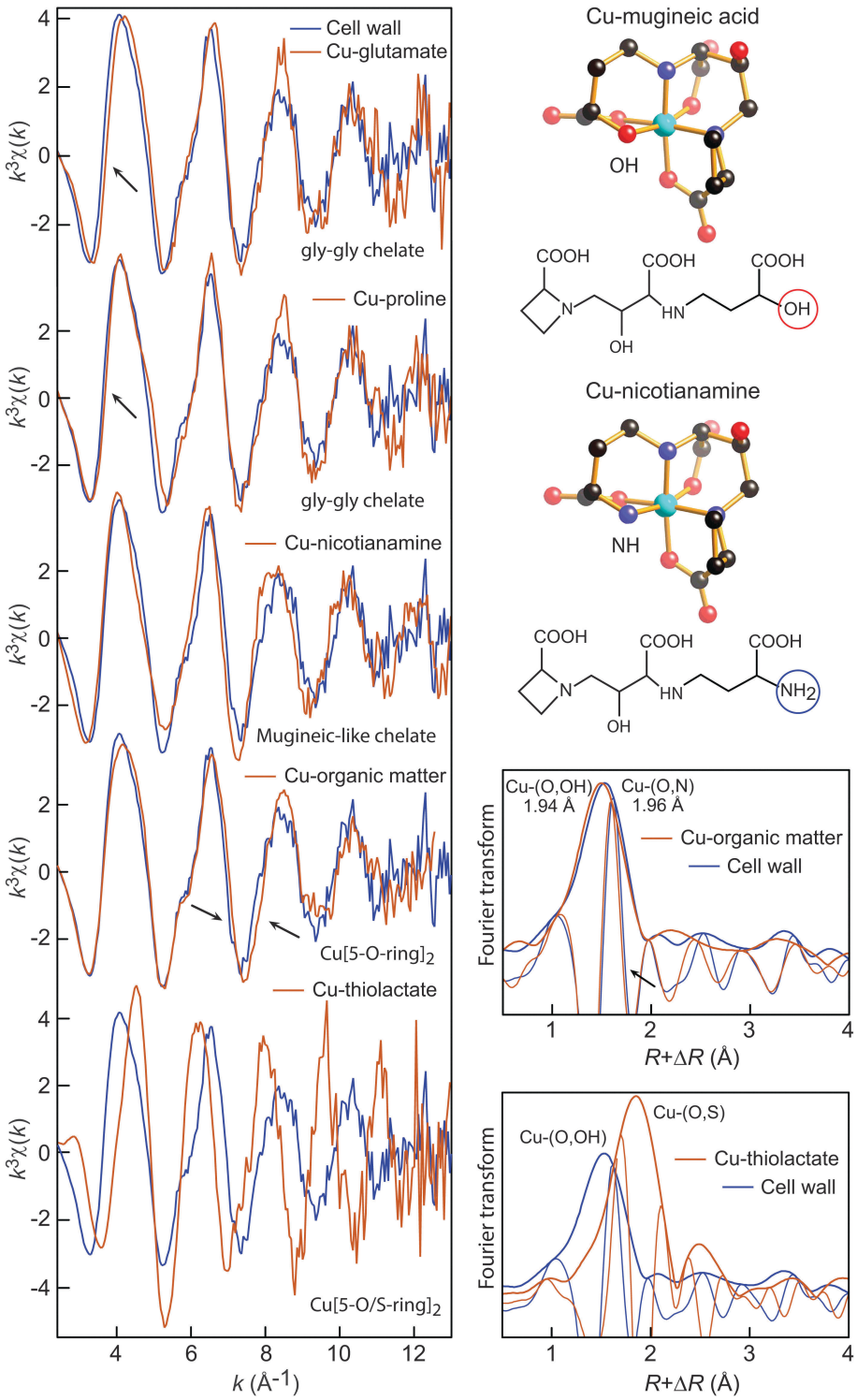

Fig. 5 EXAFS spectra of the cell wall, Cu–glutamate, Cu–proline, Cu–nicotianamine, Cu–natural organic matter chelate and Cu–thiolactate (with Fourier transforms), and structural representation of the Cu–mugineic acid and Cu–nicotianamine (NA) chelates. The cell wall spectrum is distinctly different from all models. Arrows highlight spectral differences. The Cu–NOM reference is a five-membered malate-type ring chelate described by Manceau and Matynia,[65] and used here as a proxy for Cu complexed to OH and COOH functional groups from pectates. The Fourier transform shows that the cell wall species has longer Cu–ligand distances than the pectate proxy. The Cu–thiolactate complex is a reference for sulfur ligands, as observed in some plants,[21,61,79] and reported recently for roots.[82]

Cu complexes with amino acids that form five-membered gly–gly bis-chelates: Cu–glutamate and Cu–proline (Fig. 5). The cell wall spectrum is also distinct from that of Cu–nicotianamine, which forms an intramolecular hexadentate chelate, similar to mugineic acid.[83] Other types of Cu ligands evaluated as unsuitable models for Cu complexation on cell walls include

the five-membered and six-membered Cu^{2+}–(O,S) and Cu^{2+}–O chelates described previously (Fig. 5).[65] These Cu^{2+}–O chelates account for the general class of Cu[5/6-O-ring]$_{1-2}$ structures formed with OH and COOH functional groups from pectates. Copper di-thiolactate, which forms a bis-five-membered sulfhydryl–carboxyl chelate (Cu[5-O/S-ring]$_2$), was used as reference for Cu coordinated with a mixture of O and S ligands, as reported in the roots and leaves of *Larrea tridentata*,[79] and the leaves of *T. caerulescens*.[61] The cell wall spectrum most closely resembles the pH 4.8 Cu^{2+}–his spectrum (Fig. 4a), which corroborates the XANES results. The average Cu^{2+}–ligand distance is the same in the cell wall and the pH 4.8 gly–him chelate (1.96 Å), whereas it is shorter in gly–gly (1.95 Å) and longer in him–him (1.98 Å) (Fig. 4b, ESI,† Fig. S3). The cell wall has a narrower Cu–(O,N) peak than the gly–him chelate, a weak, but well-defined, contribution from an axial oxygen, and a closer Cu–C nearest shell. These three features differentiate a square-pyramidal coordination with one O_c atom in the axial position and loss of the opposite water molecule from the coordination in the aqua gly–him chelate (ESI,† Results). It follows from XANES and EXAFS that Cu^{2+} occurs on the cell wall as a five-coordinate complex in a distorted square pyramidal geometry with bidentate and tridentate L-histidine ligands. This is the first time that copper O and N ligands have been distinguished in biota by EXAFS.[80,84]

Discussion

The results from this study provide new information on the intracellular distribution and dominant molecular form of copper in plant roots at concentrations of 50–80 mg kg^{-1} DW representative of anthropogenic ecosystems. At this level, which exceeds cellular requirements, copper is concentrated in the cell wall of *T. arvense* complexed to histidine residue. Complexation to the cell wall is determined by acid–base equilibria of functional groups (carboxyl, amine, phosphate, sulfhydryl, phenol) and affinity constants expressed thermodynamically by proton (acidity) and metal binding constants (ESI†). Proline/hydroxyproline, glycine, and glutamate make up about 30–60% of the amino acid residues in structural glycoproteins from cell walls, and histidine only about 2%.[85,86] However, histidine-rich sequences are also common in metal-transporting membrane proteins, and histidine binds Cu^{2+} more strongly than the other amino acids (log K = ~18.6 *vs.* ~15–16[87–89]) and also more strongly than other metals.[90] Carboxyl-type O ligands from polysaccharides bind Cu^{2+} with lower affinity than histidine-rich glycoproteins[91] and therefore are expected to bind Cu^{2+} only at high copper concentration after saturation of reactive amino sites.[92] The polyelectrolyte polymer character of the cell wall was demonstrated experimentally with Zn and Pb which have a reverse affinity to each other for reactive phosphate and carboxyl groups.[93] So, at low copper concentrations binding to histidine is preferred with a conformation in dynamic equilibrium with the typically mild acidic conditions of the cell wall (pH 4.5–6.0[94–96]). The higher binding strength and the finite amount of histidine ligands would explain the prevalence of carboxyl-type O ligands determined by XANES above 10^4 mg kg^{-1} DW of added copper in the root of *E. splendens*.[26] Histidine likely binds Ni,[97] in addition to Cu. In contrast to Cu in root tips of *Cucumis sativus*,[82] no Cu–S bonding was detected, possibly because measurements were performed at low temperature, which prevented the reduction of Cu^{2+} to Cu^{+} followed by its artifactual complexation to sulfur ligands.[65]

The unique structure of the ambidentate L-histidine ligand elucidates the probable thermodynamic stability and kinetic reactivity of the asymmetric Cu^{2+}–$N_{am}O_cN_{am}N_{im}$ bis-chelate. On the one hand, the hydrolytically stable tridentate coordination provides additional stability over binary Cu^{2+}–amino acid complexes (gly–gly chelate),[65] which would explain the ability of proteins with histidine residues to fix copper in cell walls. A parallel can be made with the strong carboxylate complex Cu^{2+}–citrate, which also forms a stable 5- and 6-membered tridentate chelate. On the other hand, the pendant imidazole side chain is a primary anchor for copper chelation in many metalloproteins,[98] and, as such, may be important for apoplastic scavenging of copper across the root. Noncovalent histidine–protein interactions (through hydrophobicity) may promote copper transport in the apoplast through protein–protein docking. Active copper movement from one polymer molecule to another in the cell wall was attributed previously to the difference between Cu^{+} and Cu^{2+} in their affinities for diverse ligands.[91]

Conclusion

New synchrotron-based techniques were applied successfully for *in vivo* high-resolution imaging and structural characterization of metals in plants, which are pivotal in understanding metal transport and detoxification. The results explain significant aspects of Cu immobilization in roots and suggest interesting hypotheses for detoxification and transport mechanisms. They also bring up challenging questions. For instance, how is copper imaged by nano-SXRF in xylem elements translocated to the shoot in sap? Early bulk XANES and EXAFS observations on xylem exudates from metal-accumulating plants showed that Zn and Cd change speciation in the xylem sap.[99,100] Here, the Cu concentration in the diffuse areas of the xylem elements from the non-accumulating *T. arvense* was too low for *in situ* XANES measurements, but we can expect that the ability to image and also speciate metals in main plant compartments other than the cell wall will become possible as improvements in X-ray spectroscopy design continue.

Acknowledgements

Grants from the Envirhonalpes Program from the Région Rhône-Alpes and the EC2CO program of the CNRS provided support. We thank the OTHU (Field Observatory for Urban Water Management) Federation (http://www.graie.org/othu/) and the Grand Lyon Communauté Urbaine for field access, Olivier Proux for assistance on beamline FAME (BM30B) at the ESRF, and Lysiane Brocard from the Bordeaux Imaging Center

at INRA for the preparation of the ultramicrotomic sections. Two anonymous reviewers provided thoughtful comments that were used in revising the manuscript. The Advanced Light Source is supported by the Director, Office of Science, Office of Basic Energy Sciences, of the U.S. Department of Energy under Contract No. DE-AC02-05CH11231.

References

1 G. Battistuzzi, M. Borsari, G. W. Canters, L. Loschi, F. Righi and M. Sola, *J. Am. Chem. Soc.*, 1999, **121**, 501–506.
2 I. Yruela, *Funct. Plant Biol.*, 2009, **36**, 409–430.
3 R. A. Festa and D. J. Thiele, *Curr. Biol.*, 2011, **21**, R877–R883.
4 H. Märschner, *Mineral nutrition in higher plants*, Academic Press, London, 2002.
5 C. H. R. De Vos, W. M. Ten Bookum, R. Vooijs, H. Schat and L. J. De Kok, *Plant Physiol. Biochem.*, 1993, **31**, 151–158.
6 C. M. Luna, C. A. Gonzalez and V. S. Trippi, *Plant Cell Physiol.*, 1994, **35**, 11–15.
7 J. E. J. Weckx and H. M. M. Clijsters, *Physiol. Plant.*, 1996, **96**, 506–512.
8 A. W. Girotti, *J. Lipid Res.*, 1998, **39**, 1529–1542.
9 Y. F. Tan, N. O'Toole, N. L. Taylor and A. H. Millar, *Plant Physiol.*, 2010, **152**, 747–761.
10 C. Palmer and M. L. Guerinot, *Nat. Chem. Biol.*, 2009, **5**, 333–340.
11 S. Puig and L. Penarrubia, *Curr. Opin. Plant Biol.*, 2009, **12**, 299–306.
12 N. Verbruggen, C. Hermans and H. Schat, *New Phytol.*, 2009, **181**, 759–776.
13 M. Pilon, *New Phytol.*, 2011, **192**, 305–307.
14 E. A. H. Pilon-Smits, *Annu. Rev. Plant Biol.*, 2005, **56**, 15–39.
15 M. Mench, J. P. Schwitzguebel, P. Schroeder, V. Bert, S. Gawronski and S. Gupta, *Environ. Sci. Pollut. Res.*, 2009, **16**, 876–900.
16 H. Nishizono, H. Ichikawa, S. Suziki and F. Ishii, *Plant Soil*, 1987, **101**, 15–20.
17 M. Sela, E. Telor, E. Fritz and A. Huttermann, *Plant Physiol.*, 1988, **88**, 30–36.
18 G. R. MacFarlane and M. D. Burchett, *Aquat. Bot.*, 2000, **68**, 45–59.
19 I. Brunner, J. Luster, M. S. Günthardt-Goerg and B. Frey, *Environ. Pollut.*, 2008, **152**, 559–568.
20 M. D. Vazquez, J. Barcelo, C. Poschenrieder, J. Madico, P. Hatton and A. J. M. Baker, *Bot. Acta*, 1994, **107**, 243–250.
21 D. E. Salt, R. C. Prince and I. J. Pickering, *Microchem. J.*, 2002, **71**, 255–259.
22 M. R. Broadley, P. J. White, J. P. Hammond, I. Zelko and A. Lux, *New Phytol.*, 2007, **173**, 677–702.
23 D. N. Neumann, U. Zurnieden, O. Lichtenberger and I. Leopold, *J. Plant Physiol.*, 1995, **146**, 704–717.
24 H. Y. Peng, X. E. Yang, L. Y. Jiang and Z. L. He, *J. Environ. Sci. Health, Part A*, 2005, **40**, 839–856.
25 C. Y. Ni, Y. X. Chen, Q. Lin and G. M. Tian, *J. Environ. Sci.*, 2005, **17**, 452–456.
26 J. Shi, B. Wu, X. Yuan, Y. Y. Cao, X. Chen, Y. Chen and T. Hu, *Plant Soil*, 2008, **302**, 163–174.
27 A. Manceau, K. L. Nagy, M. A. Marcus, M. Lanson, N. Geoffroy, T. Jacquet and T. Kirpichtchikova, *Environ. Sci. Technol.*, 2008, **42**, 1766–1772.
28 P. J. White, S. N. Whiting, A. J. M. Baker and M. R. Broadley, *New Phytol.*, 2002, **153**, 199–211.
29 C. W. A. do Nascimento and B. S. Xing, *Sci. Agri.*, 2006, **63**, 299–311.
30 I. Zelko, A. Lux and K. Czibula, *Int. J. Environ. Pollut.*, 2008, **33**, 123–132.
31 B. Frey, I. Brunner, P. Walter, C. Scheidegger and K. Zierold, *Plant, Cell Environ.*, 1997, **20**, 929–937.
32 G. Hause, J. Samaj, D. Menzel and F. Baluska, *Plant Signaling Behav.*, 2006, **1**, 134–139.
33 A. Carmona, G. Devès, S. Roudeau, P. Cloetens, S. Bohic and R. Ortega, *ACS Chem. Neurosci.*, 2010, **1**, 194–203.
34 I. Hurbain and M. Sachse, *Biol. Cell.*, 2011, **103**, 405–420.
35 E. Harada, A. Hokura, I. Nakai, Y. Terada, K. Baba, K. Yazaki, M. Shiono, N. Mizunog and T. Mizunoh, *Metallomics*, 2011, **3**, 1340–1346.
36 D. Zimmer, J. Kruse, C. Baum, C. Borca, M. Laue, G. Hause, R. Meissner and P. Leinweber, *Sci. Total Environ.*, 2011, **409**, 4094–4100.
37 A. Manceau, M. A. Marcus and N. Tamura, in *Applications of Synchrotron Radiation in Low-Temperature Geochemistry and Environmental Science*, ed. P. A. Fenter, M. L. Rivers, N. C. Sturchio and S. R. Sutton, Mineralogical Society of America, Washington DC, 2002, vol. 49, pp. 341–428.
38 G. N. George, I. J. Pickering, M. J. Pushie, K. Nienaber, M. J. Hackett, I. Ascone, B. Hedman, K. O. Hodgson, J. B. Aitken, A. Levina, C. Glover and P. A. Lay, *J. Synchrotron Radiat.*, 2012, **19**, 875–886.
39 G. Martinez-Criado, R. Tucoulou, P. Cloetens, P. Bleuet, S. Bohic, J. Cauzid, I. Kieffer, E. Kosior, S. Laboure, S. Petitgirard, A. Rack, J. A. Sans, J. Segura-Ruiz, H. Suhonen, J. Susini and J. Villanova, *J. Synchrotron Radiat.*, 2012, **19**, 10–18.
40 M. A. Marcus, A. A. MacDowell, R. Celestre, A. Manceau, T. Miller, H. A. Padmore and R. E. Sublett, *J. Synchrotron Radiat.*, 2004, **11**, 239–247.
41 H. Konno, T. Nakato, S. Nakashima and K. Katoh, *J. Exp. Bot.*, 2005, **56**, 1923–1931.
42 H. Konno, S. Nakashima and K. Katoh, *J. Plant Physiol.*, 2010, **167**, 358–364.
43 M. Krzesowska, *Acta Physiol. Plant.*, 2011, **33**, 35–51.
44 M. Saulais, J. P. Bedell and C. Delolme, *Water Sci. Technol.*, 2011, **64**, 255–262.
45 M. Saulais, *Colonisation végétale des bassins d'infiltration et de rétention. Caractérisation de la flore et évolution des caractéristiques physico-chimiques de l'horizon de surface végétalisé*, PhD thesis, Institut National des Sciences Appliquées de Lyon, 2011.
46 J. R. Graney and T. M. Eriksen, *Appl. Geochem.*, 2004, **19**, 1177–1188.
47 H. Li and J. Chang, *J. Environ. Eng. (Resten, Va.)*, 2012, **138**, 588–593.

48 MOE, 0-7729-9248-7, Toronto, Ontario, Canada, 1993.
49 NYSDEC New York State Department of Environmental Conservation Department of Fish Wildlife and Marine Resources, Albany NY, 1999.
50 Y. Luo, X. J. Jiang, L. H. Wu, J. Song, S. C. Wu, R. H. Lu and P. Christie, *Geoderma*, 2003, **115**, 113–120.
51 K. Demirevska-Kepova, L. Simova-Stoilova, Z. Stoyanova, R. Holzer and U. Feller, *Environ. Exp. Bot.*, 2004, **52**, 253–266.
52 A. Michaud, M. N. Bravin, M. Galleguillos and P. Hinsinger, *Plant Soil*, 2007, **298**, 99–111.
53 J. Shi, A. D. Abid, I. M. Kennedy, K. R. Hristova and W. K. Silk, *Environ. Pollut.*, 2011, **159**, 1277–1282.
54 K. Opdenakker, T. Remans, E. Keunen, J. Vangronsveld and A. Cuypers, *Environ. Exp. Bot.*, 2012, **83**, 53–61.
55 T. Punshon, M. L. Guerinot and A. Lanzirotti, *Ann. Bot.*, 2009, **103**, 665–672.
56 S. Carrasco-Gil, A. Alvarez-Fernandez, J. Sobrino-Plata, R. Millan, R. O. Carpena-Ruiz, D. L. Leduc, J. C. Andrews, J. Abadia and L. E. Hernandez, *Plant, Cell Environ.*, 2011, **34**, 778–791.
57 E. Lombi, K. G. Scheckel and I. M. Kempson, *Environ. Exp. Bot.*, 2011, **72**, 3–17.
58 S. Bohic, M. Cotte, M. Salome, B. Fayard, M. Kuehbacher, P. Cloetens, G. Martinez-Criado, R. Tucoulou and J. Susini, *J. Struct. Biol.*, 2012, **177**, 248–258.
59 B. Wu and J. S. Becker, *Metallomics*, 2012, **4**, 403–416.
60 E. Donner, T. Punshon, M. L. Guerinot and E. Lombi, *Anal. Bioanal. Chem.*, 2012, **402**, 3287–3298.
61 A. Mijovilovich, B. Leitenmaier, W. Meyer-Klaucke, P. M. H. Kroneck, B. Götz and H. Küpper, *Plant Physiol.*, 2009, **151**, 715–731.
62 V. A. Sole, E. Papillon, M. Cotte, P. Walter and J. Susini, *Spectrochim. Acta, Part B*, 2007, **62**, 63–68.
63 I. Llorens, E. Lahera, W. Delnet, O. Proux, A. Braillard, J. L. Hazemann, A. Prat, D. Testemale, Q. Dermigny, F. Gelebart, M. Morand, A. Shukla, N. Bardou, O. Ulrich, S. Arnaud, J. F. Berar, N. Boudet, B. Caillot, P. Chaurand, J. Rose, E. Doelsch, P. Martin and P. L. Solari, *Rev. Sci. Instrum.*, 2012, **83**, 063104.
64 J. G. Mesu, A. M. Beale, F. M. F. de Groot and B. M. Weckhuysen, *J. Phys. Chem. B*, 2006, **110**, 17671–17677.
65 A. Manceau and A. Matynia, *Geochim. Cosmochim. Acta*, 2010, **74**, 2556–2580.
66 L. Y. Jiang, X. E. Yang, W. Y. Shi, Z. Q. Ye and Z. L. He, *J. Plant Nutr.*, 2004, **27**, 2067–2083.
67 W. K. Silk, D. G. Bambic, R. E. O'Dell and P. G. Green, *Environ. Pollut.*, 2006, **144**, 783–789.
68 L. Q. Lou, Z. G. Shen and X. D. Li, *Environ. Exp. Bot.*, 2004, **51**, 111–120.
69 J. Song, F. J. Zhao, Y. M. Luo, S. P. McGrath and H. Z. Zhang, *Environ. Pollut.*, 2004, **128**, 307–315.
70 J. A. Qureshi, D. A. Thurman, K. Hardwick and H. A. Collin, *New Phytol.*, 1985, **100**, 429–434.
71 M. M. Lasat, A. J. M. Baker and L. V. Kochian, *Plant Physiol.*, 1996, **112**, 1715–1722.
72 A. G. L. Assunçao, P. D. Martins, S. De Folter, R. Vooijs, H. Schat and M. G. M. Aarts, *Plant, Cell Environ.*, 2001, **24**, 217–226.
73 S. A. Sinclair and U. Kraemer, *Biochim. Biophys. Acta, Mol. Cell Res.*, 2012, **1823**, 1553–1567.
74 J. Shi, M. A. Gras and W. K. Silk, *Planta*, 2009, **229**, 945–954.
75 F. C. Lidon and F. S. Henriques, *Aust. J. Plant Physiol.*, 1994, **21**, 427–436.
76 D. Liu and I. Kottke, *Bioresour. Technol.*, 2004, **94**, 153–158.
77 L. S. Kau, D. J. Spira-Solomon, J. E. Penner-Hahn, K. O. Hodgson and E. I. Solomon, *J. Am. Chem. Soc.*, 1987, **109**, 6433–6442.
78 J. G. Mesu, T. Visser, F. Soulimani, E. E. van Faassen, P. de Peinder, A. M. Beale and B. M. Weckhuysen, *Inorg. Chem.*, 2006, **45**, 1960–1971.
79 L. A. Polette, J. L. Gardea-Torresdey, R. R. Chianelli, G. N. George, I. J. Pickering and J. Arenas, *Microchem. J.*, 1998, **65**, 227–236.
80 H. Küpper, B. Götz, A. Mijovilovich, F. C. Küpper and W. Meyer-Klaucke, *Plant Physiol.*, 2009, **151**, 702–714.
81 P. M. Kopittke, N. W. Menzies, M. D. de Jonge, B. A. McKenna, E. Donner, R. I. Webb, D. J. Paterson, D. L. Howard, C. G. Ryan, C. J. Glover, K. G. Scheckel and E. Lombi, *Plant Physiol.*, 2011, **156**, 663–673.
82 J. Song, Y. Q. Yang, S. H. Zhu, G. C. Chen, X. F. Yuan, T. T. Liu, X. H. Yu and J. Y. Shi, *Biol. Plant.*, 2013, **57**, 581–586.
83 K. Nomoto, Y. Mino, T. Ishida, H. Yoshioka, N. Ota, M. Inoue, S. Takagi and T. Takemoto, *J. Chem. Soc., Chem. Commun.*, 1981, **7**, 338–339.
84 S. V. Sahi, M. Israr, A. K. Srivastava, J. L. Gardea-Torresdey and J. G. Parsons, *Chemosphere*, 2007, **67**, 2257–2266.
85 A. M. Showalter, *Plant Cell*, 1993, **5**, 9–23.
86 J. Zeier, A. Goll, M. Yokoyama, I. Karahara and L. Schreiber, *Plant, Cell Environ.*, 1999, **22**, 271–279.
87 P. M. May, P. W. Linder and D. R. Williams, *J. Chem. Soc., Dalton Trans.*, 1977, 588–595.
88 Y. Altun and F. Köseoglu, *J. Solution Chem.*, 2005, **34**, 213–231.
89 C. Curie, G. Cassin, D. Couch, F. Divol, K. Higuchi, M. Jean, J. Misson, A. Schikora, P. Czernic and S. Mari, *Ann. Bot.*, 2009, **103**, 1–11.
90 N. E. Grossoehme, S. Akilesh, M. L. Guerinot and D. E. Wilcox, *Inorg. Chem.*, 2006, **45**, 8500–8508.
91 S. C. Fry, J. G. Miller and J. C. Dumville, *Plant Soil*, 2002, **247**, 57–67.
92 T. Karlsson, K. Elgh-Dalgren and U. Skyllberg, *Soil Sci. Soc. Am. J.*, 2008, **72**, 1286–1291.
93 G. Sarret, A. Manceau, L. Spadini, J. C. Roux, J. L. Hazemann, Y. Soldo, L. Eybert-Bérard and J. J. Menthonnex, *Environ. Sci. Technol.*, 1998, **32**, 1648–1655.
94 S. C. Fry, *Biochem. J.*, 1998, **332**, 507–515.
95 J. M. Fasano, S. J. Swanson, E. B. Blancaflor, P. E. Dowd, T. H. Kao and S. Gilroy, *Plant Cell*, 2001, **13**, 907–921.

96 D. J. Cosgrove, *Nat. Rev. Mol. Cell Biol.*, 2005, **6**, 850–861.
97 M. W. Persans, X. Yan, J. M. M. L. Patnoe, U. Krämer and D. E. Salt, *Plant Physiol.*, 1999, **121**, 1117–1126.
98 R. H. Holm, P. Kennepohl and E. I. Solomon, *Chem. Rev.*, 1996, **96**, 2239–2314.
99 D. E. Salt, R. C. Prince, I. J. Pickering and I. Raskin, *Plant Physiol.*, 1995, **109**, 1427–1433.
100 D. E. Salt, R. C. Prince, A. J. M. Baker, I. Raskin and I. J. Pickering, *Environ. Sci. Technol.*, 1999, **33**, 713–717.
101 L. Schreiber, K. Hartmann, M. Skrabs and J. Zeier, *J. Exp. Bot.*, 1999, **50**, 1267–1280.
102 E. P. Colangelo and M. L. Guerinot, *Curr. Opin. Plant Biol.*, 2006, **9**, 322–330.
103 P. Deschamps, P. P. Kulkami and B. Sarkar, *Inorg. Chem.*, 2004, **43**, 3338–3340.